Entropy Measurement of a Strongly Coupled Quantum Dot

Timothy Child,[1,2,*] Owen Sheekey,[1,2] Silvia Lüscher,[1,2] Saeed Fallahi,[3,4] Geoffrey C. Gardner,[4,5] Michael Manfra,[3,4,6,5] Andrew Mitchell,[7,8] Eran Sela,[9] Yaakov Kleeorin,[10] Yigal Meir,[11,12] and Joshua Folk[1,2,†]

[1]*Stewart Blusson Quantum Matter Institute, University of British Columbia, Vancouver, British Columbia, V6T1Z4, Canada*
[2]*Department of Physics and Astronomy, University of British Columbia, Vancouver, British Columbia, V6T1Z1, Canada*
[3]*Department of Physics and Astronomy, Purdue University, West Lafayette, Indiana 47907, USA*
[4]*Birck Nanotechnology Center, Purdue University, West Lafayette, Indiana 47907, USA*
[5]*School of Materials Engineering, Purdue University, West Lafayette, Indiana 47907, USA*
[6]*Elmore Family School of Electrical and Computer Engineering, Purdue University, West Lafayette, Indiana 47907, USA*
[7]*School of Physics, University College Dublin, Belfield, Dublin 4, Ireland*
[8]*Centre for Quantum Engineering, Science, and Technology, University College Dublin, Dublin 4, Ireland*
[9]*Raymond and Beverly Sackler School of Physics and Astronomy, Tel-Aviv University, IL-69978 Tel Aviv, Israel*
[10]*Center for the Physics of Evolving Systems, University of Chicago, Chicago, Illinois 60637, USA*
[11]*Department of Physics, Ben-Gurion University of the Negev, Beer Sheva 84105, Israel*
[12]*The Ilse Katz Institute for Nanoscale Science and Technology, Ben-Gurion University of the Negev, Beer Sheva 84105, Israel*

(Received 27 April 2022; accepted 28 October 2022; published 22 November 2022)

The spin 1/2 entropy of electrons trapped in a quantum dot has previously been measured with great accuracy, but the protocol used for that measurement is valid only within a restrictive set of conditions. Here, we demonstrate a novel entropy measurement protocol that is universal for arbitrary mesoscopic circuits and apply this new approach to measure the entropy of a quantum dot hybridized with a reservoir. The experimental results match closely to numerical renormalization group (NRG) calculations for small and intermediate coupling. For the largest couplings investigated in this Letter, NRG calculations predict a suppression of spin entropy at the charge transition due to the formation of a Kondo singlet, but that suppression is not observed in the experiment.

DOI: 10.1103/PhysRevLett.129.227702

Entropy is a powerful tool for identifying exotic quantum states that may be difficult to distinguish by more standard metrics, like conductance. For example, bulk entropic signatures in twisted bilayer graphene indicate that carriers in some phases with metallic conductivity retain their local moments, as would normally be associated with a Mott insulator [1–3]. Entropy has also been proposed as a tell-tale characteristic of isolated non-Abelian quasiparticles, whether Majorana modes in a superconductor [4,5] or excitations of a fractional quantum Hall state [6–8], distinguishing them from Abelian analogs.

Quantifying the entropy of single quasiparticles is challenging due to the small signal size, of order k_B, but first steps in this direction have been made in recent years [9,10]. Reference [9] employed Maxwell relations to measure the $k_B \ln(2)$ spin entropy of a single electron confined to a quantum dot (QD) in GaAs via the temperature-induced shift of a Coulomb blockade charge transition. That approach relied on the assumption of weak coupling between the QD and the reservoirs to fit based on the specific charging line shape known for that regime. In that weak-coupling regime, spin states are pristine enough to serve as spin qubits [11–17] but the underlying physics is very simple.

The weak-coupling approach of Ref. [9] is not applicable to a broad class of mesoscopic devices [18], which limits its value in probing the complex Hamiltonians that may be implemented in such systems. For example, a single-impurity Kondo effect may be realized when the localized spin is strongly coupled to a reservoir [19,20]. Recently, more complicated structures including multiple dots have been engineered to host multichannel Kondo states [21,22], or a three-particle simulation of the Hubbard model [23]. Entropy measurements made on any of these systems would offer a significant advance in their understanding.

Here, we develop a universal protocol for mesoscopic entropy measurement that forgoes the simplifying assumptions of Ref. [9], then apply it to investigate the entropy of the first electron as it enters a quantum dot when strongly hybridized with a reservoir. The protocol is based on a Maxwell relation appropriate for mesoscopic systems, where the free energy includes both local and global terms. Expressed in integral form, the relation

$$\Delta S_{\epsilon_1 \to \epsilon_2} = -\int_{\epsilon_1}^{\epsilon_2} \frac{dN(\epsilon)}{dT} d\epsilon, \tag{1}$$

provides access to the entropy change, ΔS, of the QD-lead system as a function of the gate-tuned QD energy ϵ, based

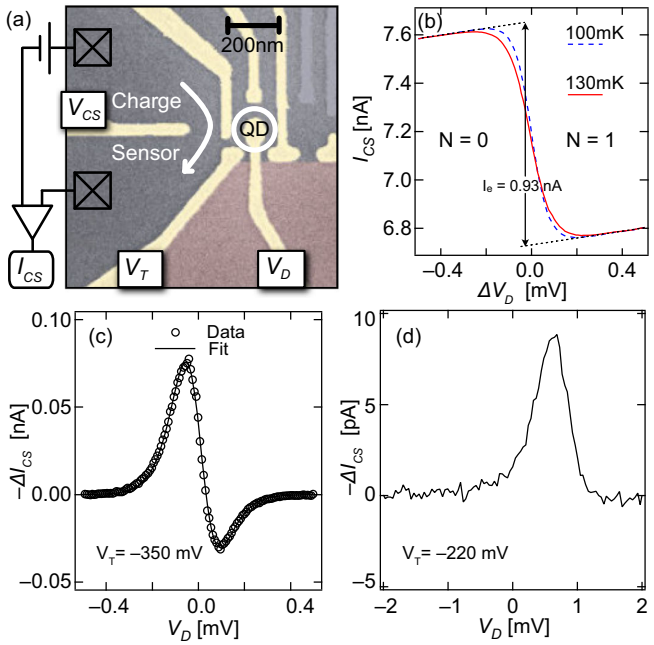

FIG. 1. (a) Scanning electron micrograph of the device. Electrostatic gates (gold) define the circuit. Squares represent Ohmic contacts to the 2DEG. The thermal electron reservoir (red) was alternated between base and elevated temperatures. (b) Current through the charge sensor, I_{CS}, for the $0 \to 1$ charge transition in a weakly coupled regime, separated into the unheated (100 mK) and heated (130 mK) parts of the interlaced measurement [25], showing the single electron step height I_e. (c), (d) Change in I_{CS} from 100 to 130 mK, for weak (c) and strong (d) coupling between QD and reservoir. (c) includes fit to weakly coupled theory.

on measurements of the change in average QD occupation, N, with temperature, T [5,18,24]. Equation (1) is related to the more conventional Maxwell relation, $\partial s/\partial \mu = \partial n/\partial T$, that applies to macroscopic systems with particle density n and entropy density s, here replacing the reservoir chemical potential μ with the dot energy ϵ [24].

We first confirm that the data match well to single-particle approximations when the coupling, Γ, between dot and reservoir is weak ($\Gamma \ll k_B T$), then show that the onset of entropy as the electron enters the dot is strongly modified when $\Gamma \gtrsim k_B T$. The measurement of this modified entropy signature is the primary result of this Letter, offering clear entropic evidence of the effect of strong reservoir coupling on the quantum state.

Measurements were performed on a mesoscopic circuit [Fig. 1(a)] in a GaAs 2D electron gas [24,25], including the QD, a charge sensing quantum point contact, and an electron reservoir that can be rapidly Joule heated above the chip temperature T to an elevated $T + \Delta T$. Coupling between the QD and the thermal reservoir is via a single tunnel barrier, with Γ controlled by V_T. The QD energy ϵ was tuned using gate voltage V_D. Throughout this Letter we report V_D with respect to the midpoint of the $N = 0 \to 1$ charge transition, $\Delta V_D \equiv V_D - V_D(N = 1/2)$. N in the QD was monitored via the current, I_{CS}, through the charge sensor [Fig. 1(b)] [26], which was biased with a dc voltage typically 100μV. Changes in occupation, N, were scaled from I_{CS} using I_e, the net drop in I_{CS} across a $1e$ charge transition [24]. Figure 1(b) illustrates weakly coupled $N = 0 \to 1$ transitions at $T = 100$ mK and $T + \Delta T = 130$ mK. Throughout this Letter both T and $T + \Delta T$ were calibrated by fitting to thermally broadened charge transitions; except where noted, $T = 100$ mK with $\Delta T \sim 30$ mK. Measurements at T and $T + \Delta T$ were interlaced by alternated Joule heating of the reservoir at 25 Hz to reduce the impact of charge instability, then averaged over several sweeps across the charge transition, see Ref. [24].

Figure 1(c) shows the change in detector current from 100 to 130 mK, $\Delta I_{\mathrm{CS}}(V_D) \equiv I_{\mathrm{CS}}(T + \Delta T, V_D) - I_{\mathrm{CS}}(T, V_D)$, scanning across the $0 \to 1$ transition in the weakly coupled regime. Note that $-\Delta I_{\mathrm{CS}}$ is plotted instead of ΔI_{CS} in order to connect visually with ΔN, which increases when I_{CS} decreases. As in Ref. [9], the line shape of $\Delta I_{\mathrm{CS}}(V_D)$ in Fig. 1(c) may be fit to a noninteracting theory for thermally broadened charge transitions to extract the change in entropy across the transition, ΔS_{fit}, not requiring calibration factors or other parameters (see Ref. [9] for details). For the data in Fig. 1(c), this yields $\Delta S_{\mathrm{fit}} = (1.02 \pm 0.01) k_B \ln(2)$, where the uncertainty reflects the standard error among five consecutive measurements at slightly different V_T.

The limitation of this approach is illustrated by the very different line shape in Fig. 1(d), reflecting the $0 \to 1$ transition when the QD is strongly coupled to the reservoir. Fitting the data in Fig. 1(d) to thermally broadened theory would yield a meaningless (and incorrect) $\Delta S_{\mathrm{fit}} > 10 k_B \ln(2)$ for the entry of the spin-1/2 electron. For a quantitative extraction of entropy beyond the weakly coupled regime of Fig. 1(c), we instead follow the integral approach in Eq. (1) that makes no assumptions on the nature of the quantum state. Evaluating Eq. (1) provides a measurement of $\Delta S(\epsilon)$ that is continuous across the charge transition, rather than just comparing $N = 0$ to $N = 1$ values.

Before moving to the quantitative evaluation of entropy, we note that the different line shapes of $\Delta I_{\mathrm{CS}}(V_D)$ in Figs. 1(c) and 1(d)—the peak-dip structure in Fig. 1(c) contrasting with the simple peak in Fig. 1(d)—can be understood as representing two temperature regimes for the Anderson impurity model. Figure 1(c) represents the high temperature limit, where dN/dT is approximately a measure of the energy derivative of the density of states in the QD, and thus exhibits positive and negative lobes. At sufficiently low temperatures, the exact solution [27] and the resulting Fermi liquid theory [28] predict a positive dN/dT for all values of the chemical potential, from the empty level to the Kondo regime through the mixed-valence regime, with a peak expected at a chemical potential corresponding to $T_K(\epsilon) \sim T$, where the entropy is expected to crossover from $S = 0$ to $S = k_B \ln(2)$. Figure 1(d),

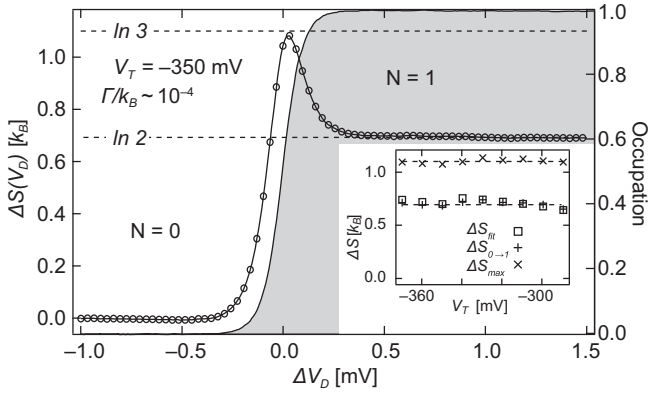

FIG. 2. Change of S in the QD across the $N = 0 \to 1$ transition, obtained by integrating $\Delta I_{CS}(V_D)$ [Fig. 1(c)] following Eq. (1). Dot occupation across the transition is shown in grey. Data obtained in the weakly coupled limit, $V_T = -350$ mV corresponding to $\Gamma/k_BT \sim 1 \times 10^{-4}$. $\Delta S_{0\to1} = (0.99 \pm 0.02)k_B \ln(2)$ is the net change ΔS across the complete transition. Inset: comparison of ΔS_{fit}, $\Delta S_{0\to1}$, and $\Delta S_{\max}$ (see text) for V_T covering approximately $10^{-5} < \Gamma/k_BT < 10^{-1}$.

corresponding to a measurement where $T \ll \Gamma$, demonstrates such all-positive dN/dT.

We next describe the evaluation of Eq. (1) from experimental data. $dN(\epsilon)/dT$ is approximated by the ratio $\Delta N(V_D)/\Delta T = -\Delta I_{CS}(V_D)/(I_e \Delta T)$. ΔT is expressed in units of gate voltage using the corresponding lever arm [24] so that the integral may be evaluated over V_D, giving $\Delta S(V_D)$. We begin by confirming the integral approach in the weakly-coupled ($\Gamma \ll k_BT$) regime, where the physics is simple.

Figure 2 shows the entropy change across the $N = 0 \to 1$ charge transition for such a weakly coupled transition, calculated from the data in Fig. 1(c) using Eq. (1). The resulting $\Delta S(\epsilon)$ indicates that the change in dot entropy is nonmonotonic as the first electron is added, reaching a $k_B \ln(3)$ peak before settling to $k_B \ln(2)$. The $k_B \ln(3)$ peak just above $\Delta V_D = 0$ reflects a combination of charge and spin degeneracy in the middle of the charge transition, with three microstates $\{|N = 0\rangle, |N = 1, \uparrow\rangle, |N = 1, \downarrow\rangle\}$ all equally probable. Charge degeneracy is gone after the transition, but spin degeneracy remains, leaving two microstates $\{|N = 1, \uparrow\rangle, |N = 1, \downarrow\rangle\}$. The net change in entropy from beginning to end, $\Delta S_{0\to1} = (0.99 \pm 0.02)k_B \ln(2)$, is nearly identical to the $\Delta S_{\text{fit}} = (1.02 \pm 0.01)k_B \ln(2)$ from Fig. 1(c), despite different sources of error for the two approaches.

The inset to Fig. 2 compares the fit and integral approaches for weakly coupled charge transitions covering 4 orders of magnitude in Γ, tuned by V_T [see Fig. 3(b) inset for calibration of Γ]. The consistency between $\Delta S_{0\to1}$ and ΔS_{fit} over the full range of weakly coupled V_T, in addition to the fact that $\Delta S_{\max}$ remains $k_B \ln(3)$ throughout this regime, confirms the accuracy of the integral approach. Small deviations from $\Delta S_{0\to1} = \Delta S_{\text{fit}} = k_B \ln(2)$, such as

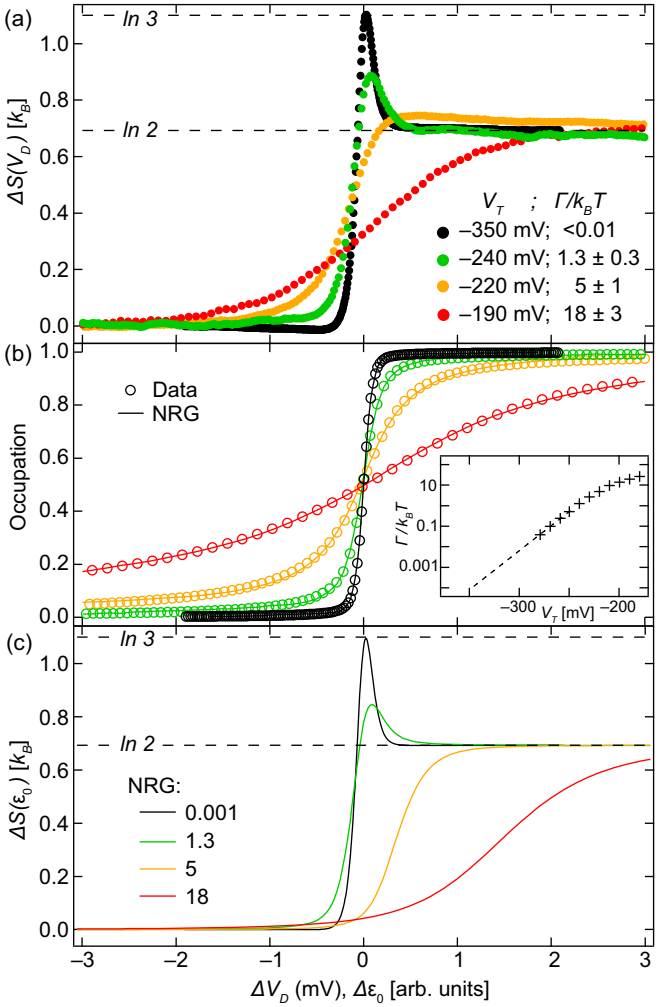

FIG. 3. Evolution of $S(\epsilon)$ from the weak (black) to strong (red) coupling regimes, comparing data [panel (a)] to NRG calculations [panel (c)]. Measurements of occupation across the charge transition are fit to NRG calculations [panel (b)], leaving no free fit parameters for the $S(\epsilon_0)$ calculation. Panel (b) inset: coupling strength of the QD to the reservoir, Γ/k_BT, extracted from fits, across the full range of V_T. Values $\Gamma/k_BT \ll 1$ cannot be measured directly and are extrapolated (dashed line).

that seen around $V_T = -330$ mV, are repeatable but sensitive to fine-tuning of all the dot gates; we believe they are due to extrinsic degrees of freedom capacitively coupled to the dot occupation, such as charge instability in shallow dopant levels in the GaAs heterostructure.

After confirming the accuracy of Eq. (1) in the weakly coupled regime, we turn to the regime $\Gamma \gtrsim k_BT$ ($V_T > -280$ mV), where the influence of hybridization is expected to emerge. Figure 3 shows the crossover from $\Gamma \ll k_BT$ to $\Gamma \gg k_BT$, illustrating several qualitative features. The $k_B \ln(3)$ peak in $\Delta S(\mu)$ decreases with Γ, until no excess entropy is visible at the charge degeneracy point for $\Gamma/k_BT \gtrsim 5$ [Fig. 3(a)]. This suppression of the entropy associated with charge degeneracy originates from the broadening by Γ of the $N = 1$ level due to hybridization with the continuous density

of states in the reservoir [5]. At the same time, the total entropy change $\Delta S_{0\to 1}$ remains $\sim k_B \ln(2)$ over the entire range of Γ explored in this experiment, reflecting the entropy of the spin-1/2 electron trapped in the QD.

To make quantitative comparison between theory and experiment, we employ numerical renormalization group (NRG) simulations [29,30] that yield N as a function of T and ϵ_0, where $-\epsilon_0$ is the depth of the dot level below the reservoir chemical potential μ. From $N(T,\epsilon_0)$, dN/dT and thereby ΔS are extracted via Eq. (1). To make a direct comparison with the experiment, $\Delta\epsilon_0 \equiv \epsilon_0 - \epsilon_0(N=1/2)$ is defined like ΔV_D, centred with respect to the charge transition. NRG parameters are calibrated to match those in the measurements by aligning the occupation $N(\Delta\epsilon_0)$ with the measured $N(\Delta V_D)$ [24], from which the appropriate Γ/T calculation may be selected and the precise connection between $\Delta\epsilon_0$ with ΔV_D is ensured. As seen in Fig. 3(b), the agreement between data and theory in terms of dot occupation is within the experimental resolution, giving confidence that measured and calculated ΔS may be compared directly.

Figure 3(c) illustrates NRG predictions for $\Delta S(\epsilon_0)$ over the range of Γ accessible in our measurements. Matching the data, the peak in entropy due to charge degeneracy is suppressed for $\Gamma > k_B T$, while the net entropy change across the transition remains $k_B \ln(2)$. At the same time, a qualitative difference between data and NRG calculations is the shift to the right seen in NRG curves for higher Γ [Fig. 3(c)], but not observed in the measurements [Fig. 3(a)]. This relative shift of NRG curves with respect to data is not explained by an offset of $\Delta\epsilon_0$ with respect to ΔV_D, as the two are aligned by the occupation data [Fig. 3(b)].

Instead, the shift of NRG curves to the right (to larger chemical potential) with increasing Γ is explained by the virtual exchange interactions underlying the Kondo effect, which form a quasibound singlet state between the localized spin and a cloud of delocalized spins in the reservoir at temperatures below T_K. This state has no magnetic moment [31] and, in the case of a single-electron QD, zero entropy. Thus, due to the Kondo effect, we expect the entropy to remain zero for all dot energies that obey $T < T_K(\epsilon_0)$. Since $T_K \propto e^{-\pi(\epsilon_0-\mu)/\Gamma}$ in the (experimentally relevant) large-U limit, where U represents the QD charging energy, we expect the onset of $k_B \ln(2)$ entropy to shift to larger values of ϵ as Γ increases, as seen in the NRG results.

It remains a puzzle why the strong suppression of entropy right at the charge transition, seen in NRG calculations for $\Gamma/k_B T \geq 5$, is not observed in the data. It is possible that the charge measurement itself can lead to dephasing of the Kondo singlet [32–34]. In order to test for charge-sensor dephasing in our measurement, the experiment was repeated at charge sensor biases from 300 μV down to 50 μV, but no dependence on the bias was seen in the data [24]. In the future, experiments that allow simultaneous transport and entropy characterization of the Kondo state may help to resolve this puzzle.

This project has received funding from European Research Council (ERC) under the European Union's Horizon 2020 research and innovation program under Grant Agreement No. 951541. Y. M. acknowledges discussions with A. Georges and support by the Israel Science Foundation (Grant No. 3523/2020). Experiments at UBC were undertaken with support from the Stewart Blusson Quantum Matter Institute, the Natural Sciences and Engineering Research Council of Canada, the Canada Foundation for Innovation, the Canadian Institute for Advanced Research, and the Canada First Research Excellence Fund, Quantum Materials and Future Technologies Program. S. F., G. C. G., and M. M. were supported by the US DOE Office of Basic Energy Sciences, Division of Materials Sciences and Engineering award DE-SC0006671 and QIS award DE-SC0020138. A. K. M. acknowledges funding from the Irish Research Council Laureate Awards 2017/2018 through Grant No. IRCLA/2017/169.

*timjchild@phas.ubc.ca
†jfolk@physics.ubc.ca

[1] Yu Saito, Fangyuan Yang, Jingyuan Ge, Xiaoxue Liu, Takashi Taniguchi, Kenji Watanabe, J. I. A. Li, Erez Berg, and Andrea F. Young, Isospin Pomeranchuk effect in twisted bilayer graphene, Nature (London) **592**, 220 (2021).

[2] Asaf Rozen, Jeong Min Park, Uri Zondiner, Yuan Cao, Daniel Rodan-Legrain, Takashi Taniguchi, Kenji Watanabe, Yuval Oreg, Ady Stern, Erez Berg, Pablo Jarillo-Herrero, and Shahal Ilani, Entropic evidence for a Pomeranchuk effect in magic-angle graphene, Nature (London) **592**, 214 (2021).

[3] Biao Lian, Heating freezes electrons in twisted bilayer graphene, Nature (London) **592**, 191 (2021).

[4] Sergey Smirnov, Majorana tunneling entropy, Phys. Rev. B **92**, 195312 (2015).

[5] Eran Sela, Yuval Oreg, Stephan Plugge, Nikolaus Hartman, Silvia Lüscher, and Joshua Folk, Detecting the Universal Fractional Entropy of Majorana Zero Modes, Phys. Rev. Lett. **123**, 147702 (2019).

[6] N. R. Cooper and Ady Stern, Observable Bulk Signatures of Non-Abelian Quantum Hall States, Phys. Rev. Lett. **102**, 176807 (2009).

[7] Kun Yang and Bertrand I. Halperin, Thermopower as a possible probe of non-abelian quasiparticle statistics in fractional quantum hall liquids, Phys. Rev. B **79**, 115317 (2009).

[8] G. Ben-Shach, C. R. Laumann, I. Neder, A. Yacoby, and B. I. Halperin, Detecting Non-Abelian Anyons by Charging Spectroscopy, Phys. Rev. Lett. **110**, 106805 (2013).

[9] Nikolaus Hartman, Christian Olsen, Silvia Lüscher, Mohammad Samani, Saeed Fallahi, Geoffrey C. Gardner, Michael Manfra, and Joshua Folk, Direct entropy measurement in a mesoscopic quantum system, Nat. Phys. **14**, 1083 (2018).

[10] Yaakov Kleeorin, Holger Thierschmann, Hartmut Buhmann, Antoine Georges, Laurens W. Molenkamp, and Yigal Meir, How to measure the entropy of a mesoscopic system via thermoelectric transport, Nat. Commun. **10**, 5801 (2019).
[11] J. M. Elzerman, R. Hanson, L. H. Willems van Beveren, B. Witkamp, L. M. K. Vandersypen, and L. P. Kouwenhoven, Single-shot read-out of an individual electron spin in a quantum dot, Nature (London) **430**, 431 (2004).
[12] J. R. Petta, A. C. Johnson, J. M. Taylor, E. A. Laird, A. Yacoby, M. D. Lukin, C. M. Marcus, M. P. Hanson, and A. C. Gossard, Coherent manipulation of coupled electron spins in semiconductor quantum dots, Science **309**, 2180 (2005).
[13] R. Hanson, L. P. Kouwenhoven, J. R. Petta, S. Tarucha, and L. M. K. Vandersypen, Spins in few-electron quantum dots, Ph.D. thesis, 2007.
[14] C. Barthel, D. J. Reilly, C. M. Marcus, M. P. Hanson, and A. C. Gossard, Rapid Single-Shot Measurement of a Singlet-Triplet Qubit, Phys. Rev. Lett. **103**, 160503 (2009).
[15] Hendrik Bluhm, Sandra Foletti, Diana Mahalu, Vladimir Umansky, and Amir Yacoby, Enhancing the Coherence of a Spin Qubit by Operating it as a Feedback Loop That Controls its Nuclear Spin Bath, Phys. Rev. Lett. **105**, 216803 (2010).
[16] K. C. Nowack, M. Shafiei, M. Laforest, G. E. D. K. Prawiroatmodjo, L. R. Schreiber, C. Reichl, W. Wegscheider, and L. M. K. Vandersypen, Single-shot correlations and two-qubit gate of solid-state spins, Science **333**, 1269 (2011).
[17] M. D. Shulman, O. E. Dial, S. P. Harvey, H. Bluhm, V. Umansky, and A. Yacoby, Demonstration of entanglement of electrostatically coupled singlet-triplet qubits, Science **336**, 202 (2012).
[18] Eugenia Pyurbeeva and Jan A. Mol, A thermodynamic approach to measuring entropy in a few-electron nanodevice, Entropy **23**, 640 (2021).
[19] D. Goldhaber-Gordon, Hadas Shtrikman, D. Mahalu, David Abusch-Magder, U. Meirav, and M. A. Kastner, Kondo effect in a single-electron transistor, Nature (London) **391**, 156 (1998).
[20] Michael Pustilnik and Leonid Glazman, Kondo effect in quantum dots, J. Phys. Condens. Matter **16**, R513 (2004).
[21] R. M. Potok, I. G. Rau, Hadas Shtrikman, Yuval Oreg, and D. Goldhaber-Gordon, Observation of the two-channel Kondo effect, Nature (London) **446**, 167 (2007).
[22] A. J. Keller, L. Peeters, C. P. Moca, I. Weymann, D. Mahalu, V. Umansky, G. Zaránd, and D. Goldhaber-Gordon, Universal Fermi liquid crossover and quantum criticality in a mesoscopic system, Nature (London) **526**, 237 (2015).
[23] J. P. Dehollain, U. Mukhopadhyay, V. P. Michal, Y. Wang, B. Wunsch, C. Reichl, W. Wegscheider, M. S. Rudner, E. Demler, and L. M. K. Vandersypen, Nagaoka ferromagnetism observed in a quantum dot plaquette, Nature (London) **579**, 528 (2020).
[24] See Supplemental Material at http://link.aps.org/supplemental/10.1103/PhysRevLett.129.227702 for a derivation of the Maxwell relation used in this work, as well as further device and measurement details.
[25] Timothy Child, Owen Sheekey, Silvia Lüscher, Saeed Fallahi, Geoffrey C. Gardner, Michael Manfra, and Joshua Folk, A robust protocol for entropy measurement in mesoscopic circuits, Entropy **24**, 417 (2022).
[26] M. Field, C. G. Smith, M. Pepper, D. A. Ritchie, J. E. F. Frost, G. A. C. Jones, and D. G. Hasko, Measurements of Coulomb Blockade with a Noninvasive Voltage Probe, Phys. Rev. Lett. **70**, 1311 (1993).
[27] A. M. Tsvelick and P. B. Wiegmann, Exact results in the theory of magnetic alloys, Adv. Phys. **32**, 453 (1983).
[28] Christophe Mora, Cătălin Paşcu Moca, Jan von Delft, and Gergely Zaránd, Fermi-liquid theory for the single-impurity anderson model, Phys. Rev. B **92**, 075120 (2015).
[29] O. Legeza, C. P. Moca, A. I. Toth, I. Weymann, and G. Zarand, Manual for the flexible DM-NRG code, arXiv:0809.3143.
[30] A. I. Tóth, C. P. Moca, Ö. Legeza, and G. Zaránd, Density matrix numerical renormalization group for non-Abelian symmetries, Phys. Rev. B **78**, 245109 (2008).
[31] Jun Kondo, Resistance minimum in dilute magnetic alloys, Prog. Theor. Phys. **32**, 37 (1964).
[32] M. Avinun-Kalish, Moty Heiblum, Alessandro Silva, Diana Mahalu, and V. Umansky, Controlled Dephasing of a Quantum Dot in the Kondo Regime, Phys. Rev. Lett. **92**, 156801 (2004).
[33] Alessandro Silva and Shimon Levit, Peculiarities of the controlled dephasing of a quantum dot in the Kondo regime, Europhys. Lett. **62**, 103 (2003).
[34] Kicheon Kang and Gyong Luck Khym, Entanglement, measurement, and conditional evolution of the Kondo singlet interacting with a mesoscopic detector, New J. Phys. **9**, 121 (2007).

A MESOSCOPIC MAXWELL RELATION

Our goal is to calculate the entropy change of the full thermodynamic system, including both the QD and the lead to which it is coupled, that occurs as the QD occupation is tuned by voltage applied to a local gate. This gate voltage can be modelled as a local potential ϵ for the QD occupation N; it is this quantity, which is thermodynamically conjugate to the local potential, that has to be measured with the charge detector.

We are operating under the approximation that the local gate-tuned potential couples precisely and only to the charge of the QD. Then, the differential of the grand potential Φ for the system may be written as:

$$d\Phi = -SdT - (N_{res} + N)d\mu + Nd\epsilon + ...$$

where S is the total entropy of the system, μ is the total chemical potential of the system that contains $N_{res} + N$ electrons, N_{res} is the average occupation of the reservoir, N is the average occupation of the QD level with energy ϵ, and ... represents other terms irrelevant to this calculation. Then, we have

$$\partial\Phi/\partial\epsilon = N \tag{S1}$$
$$\partial\Phi/\partial T = -S \tag{S2}$$
$$\frac{\partial^2\Phi}{\partial\epsilon\partial T} = \frac{\partial^2\Phi}{\partial T\partial\epsilon}, \text{ giving} \tag{S3}$$
$$\partial N/\partial T = -\partial S/\partial\epsilon \tag{S4}$$

which is integrated to give Eq. 1. We emphasize that the relation $\partial\Phi/\partial\epsilon = N$ only holds if there is a term, $H_{gate} = \epsilon\hat{N}$, in the gate-controlled Hamiltonian. Here $\hat{N}$ is the charge operator of the QD. We emphasize that this relation holds for the thermal averaged value $N \equiv \langle\hat{N}\rangle$, even though $\hat{N}$ is not a conserved quantity.

As well, ϵ must not couple to any other (reservoir) degrees of freedom. Although one might worry about a direct effect of V_D on the reservoir, the fact that ΔI_{CS} is zero outside of the charge transition region (see e.g. Figs 1cd, 3a) shows that any effect that is there does not modify the entropy as determined via Eq. 1.

DEVICE FABRICATION

The device was fabricated in a GaAs/AlGaAs heterostructure that hosts a 2D Electron Gas (2DEG) 57nm below the surface and that had a 300 mK carrier density of $2.42 \times 10^{11}\text{cm}^{-2}$ with mobility $2.56 \times 10^6\text{cm}^2/(\text{Vs})$. A UV laser writer was used to define the mesas, followed by electron beam lithography to define NiAuGe ohmic contacts. Additionally, 10 nm of HfO_2 was deposited by atomic layer deposition to improve gating stability. The electrostatic gates were fabricated with two stages of electron beam lithography followed by electron beam evaporation: a fine step for the inner parts, and a coarse step for the outer parts of the gates. In the fine step, 2/12 nm of Pd/Au were deposited. In the coarse step, 10/150 nm of Ti/Au were deposited.

MEASUREMENT ELECTRONICS

A custom built combined DAC/ADC unit was used to apply potentials to the gates and heating QPCs as well as to record the voltage output of a Current to Voltage Basel SP983c amplifier (https://www.baspi.ch/low-noise-high-stab-itov-conv). The DAC/ADC unit is built from an Arduino Due and two Analog Devices evaluations boards: the AD5764 DAC and AD7734 ADC. The Arduino is the interface between the measurement PC and the DAC/ADC boards. The whole design is based on the information provided at [http://opendacs.com/dac-adc-homepage/] with some substantial modifications, particularly to the Arduino code (https://github.com/folk-lab/FastDAC). The most significant modification is to provide functionality to apply a synchronized square wave bias for heating, whilst measuring continuously.

CHARGE SENSOR MAPPING

The charge sensor is tuned to the most linear regime before each measurement (Fig. S2a). In the limit of very strong coupling, however, the transition becomes so broad that the non-linearity of the charge sensor may begin to

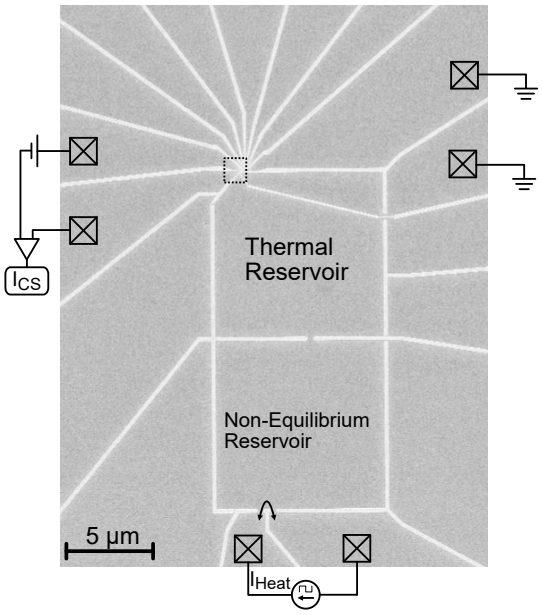

FIG. S1. Scanning electron micrograph of the larger structure of the device with a symbolic representation of connections to the device. The region shown in Fig. 1a in the main text is denoted by the dotted square. All Ohmic contacts (crossed squares) are located about 0.5 mm away. The charge sensor shown in Fig 1a is in the top left. Ohmics in the top right are grounded to ensure a fixed potential in the electron reservoirs near the dot. Electrons in the enclosed reservoirs are heated by driving an alternating square wave current through two QPCs at the bottom of the potentially non-equilibrium reservoir. Heat then diffuses to the thermal reservoir through the middle QPC, resulting in a uniformly heated electron reservoir next to the QD.

play a role. In our experiment, ΔI_{CS} is converted to ΔN assuming a linear relation between the two, but when I_{CS} is not linear in the additional electrostatic potential provided by, e.g., cross capacitance with V_D, this assumption is no longer valid.

To remove potential inaccuracy in the conversion between ΔI_{CS} and ΔN due to non-linearity, I_{CS} may be mapped back to an equivalent charge sensor gate voltage, V_{CS}, using a measurement $I_{CS}(V_{CS})$ (Fig. S2c). Performing the entropy calculation using the equivalent gate voltage, instead of I_{CS}, reduces any impact of charge sensor non-linearity in the measurement of ΔN. In practice, however, no statistically significant difference was observed in entropy calculations using the two approaches, so charge sensor mapping was not used.

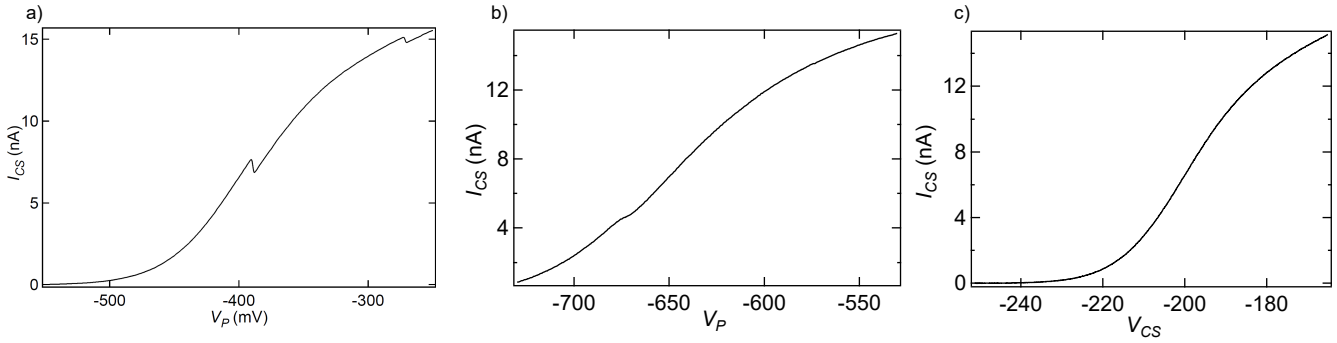

FIG. S2. a) A very wide sweep over a weakly coupled $0 \rightarrow 1$ transition using the plunger gate V_P (the gate directly above the QD in Fig. 1) showing the response of the charge sensor, and the usual alignment of the $0 \rightarrow 1$ transition at the steepest, most linear part of the charge sensor response. The second step observed near $V_P = -270$ mV is the $1 \rightarrow 2$ transition. A rough estimate of the charging energy, E_C, of the dot for the $1 \rightarrow 2$ transition may be made based on the spacing in gate voltage, giving $E_C \sim 1$ meV. b) An equivalent sweep over a strongly coupled ($\Gamma/k_BT \sim 10$) $0 \rightarrow 1$ transition at $V_P = -670$ mV (note: this specific measurement was taken without V_{CS} adjusted such that the transition occurs in the steepest, most linear part of the CS response). c) Data of charge sensor current, I_{CS}, vs the charge sensor QPC tuning gate (see Fig. 1a) used for mapping I_{CS} to a quantity in units of mV that is linear in electrostatic potential.

DETERMINING ΔS BY DIRECT FITTING OF dN/dT DATA

For systems where the addition of an electron to the charge sensed quantum dot has a simple lineshape, as in the case of a QD weakly coupled to a thermal reservoir, it is possible to extract the entropy change of the system by fitting the ΔI_{CS} data directly as was done in Ref. 9. This procedure is made possible through the application of the Maxwell relation:

$$\left(\frac{\partial \mu}{\partial T}\right)_{p,N} = -\left(\frac{\partial S}{\partial N}\right)_{p,T}$$

For a QD weakly coupled to a thermal reservoir, the charging lineshape takes the form:

$$N(V_D, \Theta) = \tanh\left(\frac{V_D - V_{mid}(\Theta)}{2\Theta}\right)$$

where $\Theta = \frac{k_B T}{\alpha e}$ and $V_{mid}(\Theta)$ is the plunger gate voltage at $N = 1/2$. V_{mid} changes the quantum dot energy level–that is, the energy required to add an electron to the dot–and therefore maps to the chemical potential μ in equilibrium.

Differentiating N with respect to T, one finds a lineshape that depends explicitly on ΔS:

$$\partial N(V_D, \Theta) \propto -\partial T\left[\frac{V_D - V_{mid}(\Theta)}{2\Theta} - \frac{\Delta S}{2k_B}\right] \times \cosh^{-2}\left(\frac{V_D - V_{mid}(\Theta)}{2\Theta}\right)$$

after substituting

$$\frac{\partial V_{mid}}{\partial \Theta} = \frac{1}{k_B}\frac{\partial \mu}{\partial T} = \frac{1}{k_B}\Delta S_{N-1\to N}$$

.

Here $\partial N(V_D, \Theta)$ is the difference in occupation of the QD for the reservoir temperature changing from $T \to T + \Delta T$. Fitting this equation to the ΔI_{CS} data, ΔS is obtained as a fit parameter independent of the scaling of the data.

FITTING NRG TO DATA

NRG calculations were carried out using the flexible DM-NRG code[28, 29] on the standard single impurity Anderson model. In the calculation, we assume infinite interaction U, a constant density of states in the reservoir with bandwidth $D = 1$ exceeding all other energy scales, and we keep 350 states per iteration with discretization constant $\Lambda = 2$. Results are given in arbitrary units of energy. Note that NRG curves are independent of the values of bandwidth, W, and of U, as long as $U, W \gg T, \Gamma$ because, as with the experimental plots, all curves are shifted such that $x = 0$ corresponds to half filling.

Our procedure for fitting the occupation, N, of NRG calculations to measured data involves three steps: 1. Linearly interpolating over the 2D array of calculations. 2. Adding terms (amplitude, constant, linear) to account for the behaviour of the charge sensor in detecting the QD occupations. 3. Allowing for an offset and scaling proportional to Θ (T in units of gate voltage) in the ϵ_0 axis. We then use Powell's method of minimization [35] to find the best fitting parameters allowing all to vary with the exception of Γ and Θ, for which only one is allowed to vary. In the weakly coupled regime, it is reasonable to approximate $\Gamma \sim 0$, and with that constraint, we are able to determine $\Theta(V_D)$. We find a linear relationship between $\Theta(V_D)$ and V_T which implies a linearly changing lever arm, α, as the system temperature, T, is fixed (Fig. S3). Note that the lever arm, α, connects Θ in units of gate voltage to temperature, T, in kelvin (Eq.S5),

$$\alpha\Theta = k_B T \tag{S5}$$

and is a measure of the strength of effect the plunger gate, V_D, has on the QD. The linear change implies that as V_T is varied, the strength of effect of V_D also varies. We attribute this to a change of shape of the QD where it moves it further from V_D for more positive V_T. For measurements into the strongly coupled regime where $\Gamma \gg 0$, we force the Θ parameter to follow the linear relationship found in the weakly coupled regime, allowing Γ to be a varying parameter. The fit parameters found by comparing N of NRG data to I_{CS} of measured data can then be used to directly compare between the NRG dN/dT calculations and ΔI_{CS} measurements.

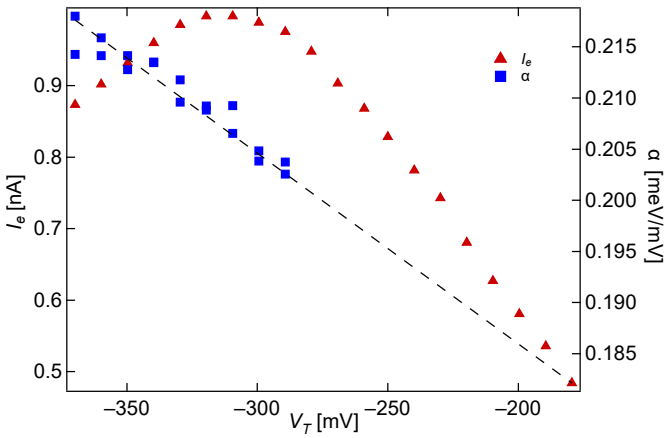

FIG. S3. Variation of lever arm α, and charge step I_e measured independently over the full range of V_T explored in this experiment. Dashed line: extrapolation of α into the strongly-coupled regime where it cannot be measured directly.

SCALING FROM ΔI_{CS} TO dN/dT

The complete procedure for scaling from ΔI_{CS} to dN/dT is comprised of two parts: Conversion of ΔI_{CS} to ΔN, and calculation of the corresponding ΔT, expressed in equivalent mV on V_D.

The procedure for scaling the ΔI_{CS} measurements to dN/dT involves scaling $\Delta I_{CS} \rightarrow \Delta N$, then dividing by ΔT as described in the main text. The $\Delta I_{CS} \rightarrow \Delta N$ conversion is a straightforward division by I_e (Fig. S3), the net change of current through the charge sensor for the addition of 1 full electron to the QD. In order to extract I_e from the data, measurements of I_{CS} are fit to NRG calculations of dot occupation across the transition, after adding a fixed offset that account for the setting of the charge sensor in the middle of its first charge step, and a linear term that accounts for cross capacitance between V_D and the charge sensor. Examples of the fixed and linear terms are seen clearly in Fig. S1a, where a very whide scan of V_P (over a much larger range than required for the charge transition) is able to completely pinch off the charge sensor, or to bring it to the first plateau. The cross capacitive effect of V_D is much smaller than that of V_P: its lever arm to the QD energy level is much larger, so much only mV or sub-mV changes are required in V_D to sweep across a charge transition.

ΔT is easily extracted in units of equivalent gate voltage (V_D) for weakly coupled V_T by fitting cold and hot occupation data to NRG. For strongly coupled transitions, however, ΔT does not result in a broadening of the transition lineshape, so it must be determined in another way. The real temperature change of the reservoir does not depend on V_T, of course, but the lever arm α does depend on V_T. We calculate $\Delta T(V_T)$ in equivalent mV on V_D by

1. fitting hot and cold transitions for a range of weakly coupled V_T, to determine both $\Delta T(V_T)$ in equivalent V_D and $\alpha(V_T)$ through this range.

2. $\alpha(V_T)$ is observed to be linear in V_T, and extrapolated to strongly-coupled V_T (dashed line in Fig. 1c, main text).

3. ΔT in equivalent V_D is calculated for strongly coupled transitions using $\alpha(V_T)$ determined above.

AVERAGING PROCEDURE

The data shown in the main text is the result of averaging measurements over many sweeps over the transition. In the strongly coupled regime, as the ΔI_{CS} signal becomes weaker, averaging data becomes particularly important. It is often necessary to measure for 10's of minutes or even hours in order to obtain a reasonable signal to noise ratio, but the presence of charge instability makes single slow measurements over the transition unreliable. By repeatedly sweeping over the transition quickly, then aligning each sweep based on a fit to the I_{CS} data before averaging, we can improve the signal to noise ratio of the corresponding ΔI_{CS} whilst mitigating the effect of charge instability. This procedure of post-aligning individual charge transition scans is followed for measurements in the range $V_T < -230$ mV.

For more strongly coupled measurements ($V_T \geq -230$ mV), determining the center of each individual scan through fitting is not reliable; as a result, data is averaged without centring first. Charge instability (determined in the weakly coupled regime) is on the order of 6 μeV without significant long-term drift seen in the data. For the most strongly coupled measurements, where the width of the transition is on the order of 400 μeV, the lack of centring therefore is expected to have a negligible effect. Occasional larger jumps in transition position (0.5 mV) do occur on a timescale of hours; care is taken never to average data across such jumps.

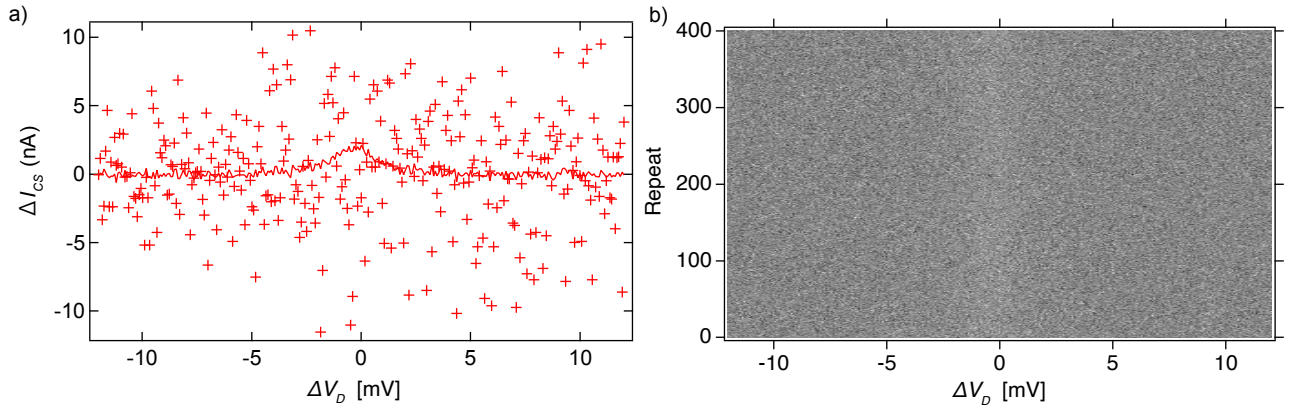

FIG. S4. a) Markers illustrate a single measurement across the charge transition, which takes 30 seconds to complete. No peak in ΔI_{CS} can be seen in this raw data. After averaging 400 of such scans together (solid line), however, a small peak in ΔI_{CS} is seen at $\Delta V_D = 0$. b) Raw ΔI_{CS} data (greyscale) for 400 scans as in panel a). Averaged together, they yield the solid line in panel a).

LACK OF DEPENDENCE ON CHARGE SENSOR BIAS

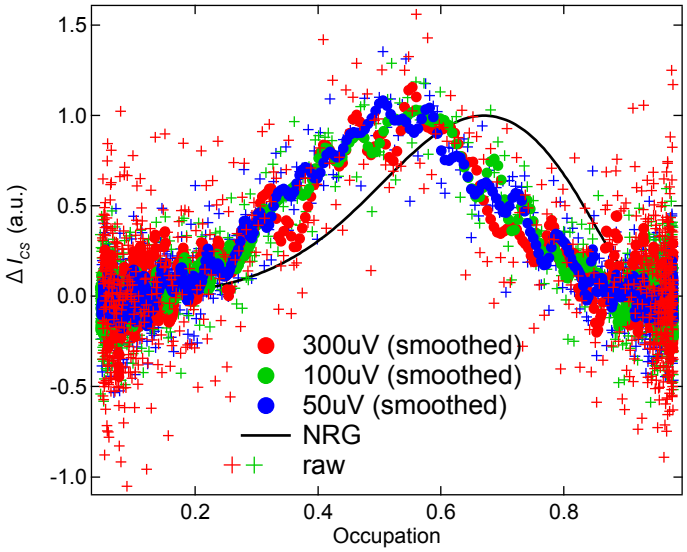

FIG. S5. The lineshape of ΔI_{CS}, here plotted vs occupation instead of V_D, shows no dependence on V_{CS} within experimental noise, though of course the magnitude of I_{CS} and ΔI_{CS} scales linearly with V_{CS}. The case of $\Gamma/k_BT = 24$ is shown here. In particular, ΔI_{CS} remains peaked at $N \sim 0.5$, in contrast to the NRG calculation (solid line) in which the shifted peak reflects the screening of spin entropy in the mixed valence regime due to the formation of the Kondo singlet.